Supporting information

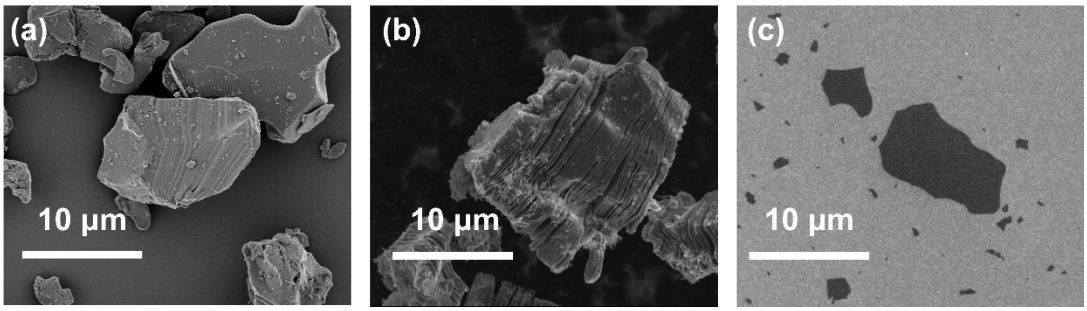

Figure S1. SEM images of the preparative process of $Ti_3C_2T_x$:(a) Ti_3AlC_2 phase. (b) Multilayer $Ti_3C_2T_x$. (c) Single-layer $Ti_3C_2T_x$ dispersion.

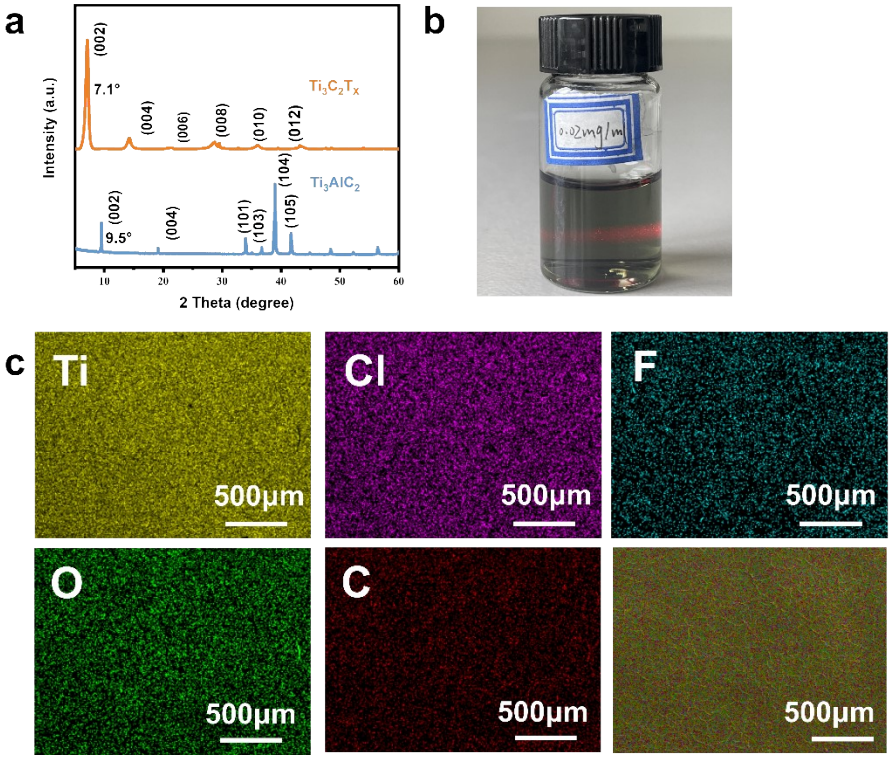

Figure S2. (a) XRD patterns of Ti_3AlC_2 phase and $Ti_3C_2T_x$. (b) Tyndall phenomenon of single-layer $Ti_3C_2T_x$ dispersion. (c) SEM mapping of $Ti_3C_2T_x$ films with Ti, C, O, F, and Cl elements.

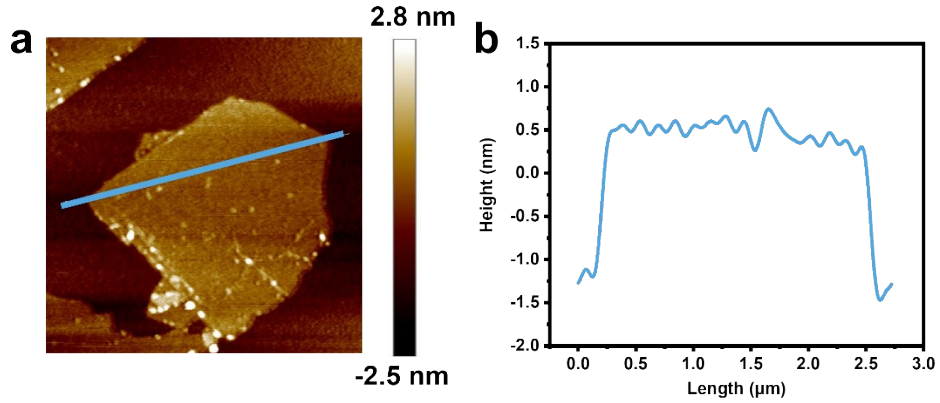

Figure S3. (a) Schematic diagram of AFM for single-layer $Ti_3C_2T_x$. (b) The thickness variation diagram of the cross-sectional position of single-layer $Ti_3C_2T_x$

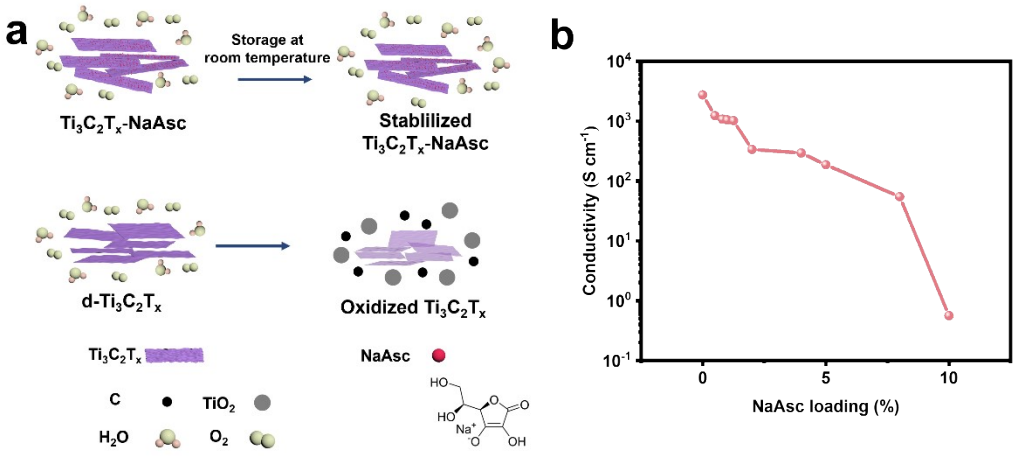

Figure S4. (a) Schematic representation of the antioxidant properties of pristine $Ti_3C_2T_x$ and $Ti_3C_2T_x$ with complexed NaAsc under aqueous-oxygen conditions. (b) Schematic representation of $Ti_3C_2T_x$ conductivity changes with increasing NaAsc content.

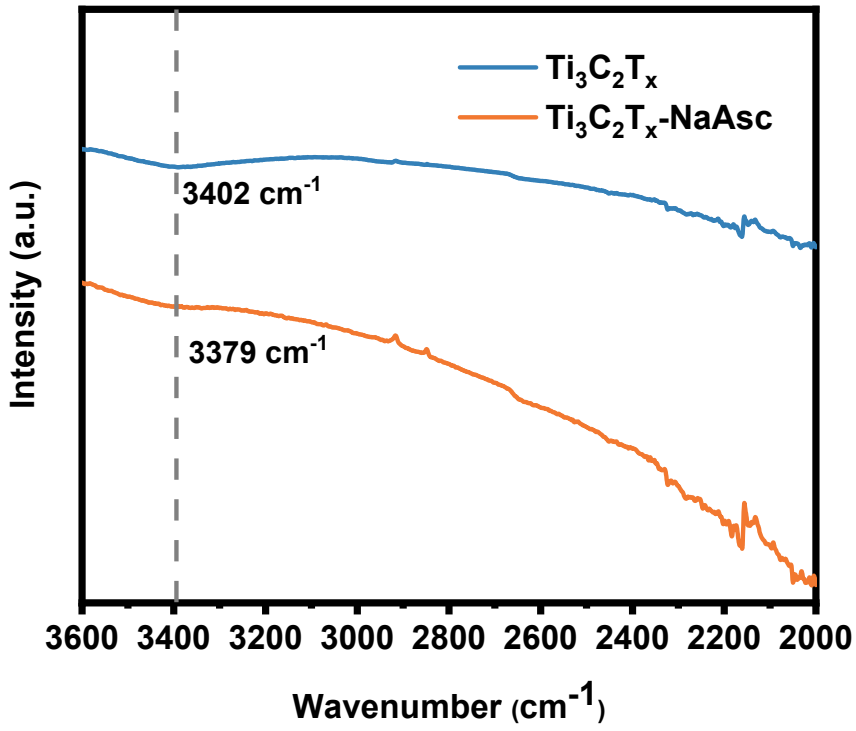

Figure S5 FTIR Analysis of $Ti_3C_2T_x$ and $Ti_3C_2T_x$-NaAsc

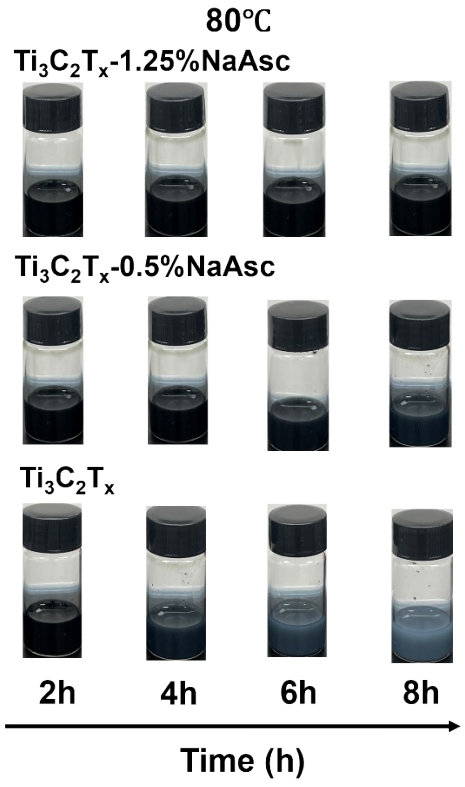

Figure S6. Optical images of $Ti_3C_2T_x$ dispersions and $Ti_3C_2T_x$-NaAsc dispersions with

different NaAsc contents showing color changes over time at 80 °C.

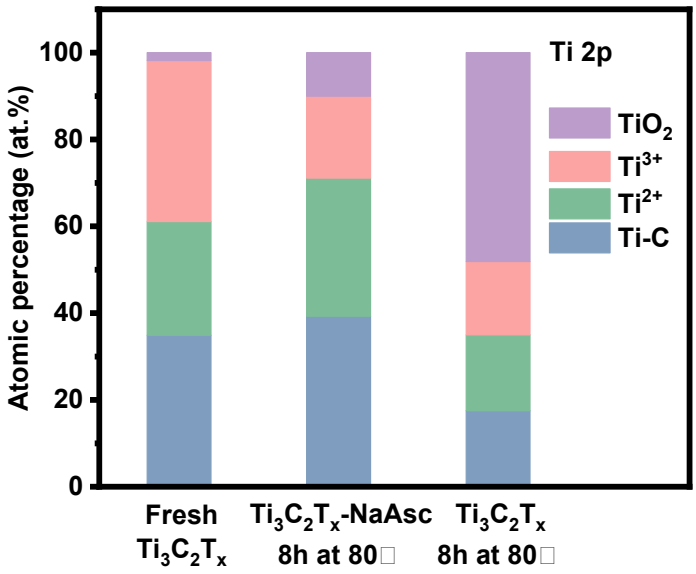

Figure S7. Atomic percentage of Ti 2p XPS peak-fitting of the original $Ti_3C_2T_x$, $Ti_3C_2T_x$ dispersion oxidized at 80°C for 8 h, and $Ti_3C_2T_x$-NaAsc dispersion.

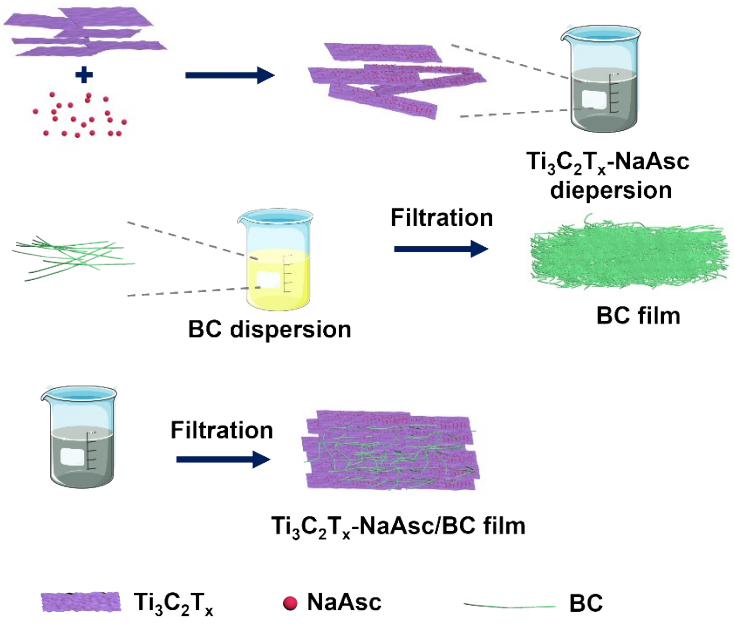

Figure S8. Schematic flow of $Ti_3C_2T_x$-NaAsc/BC film preparation.

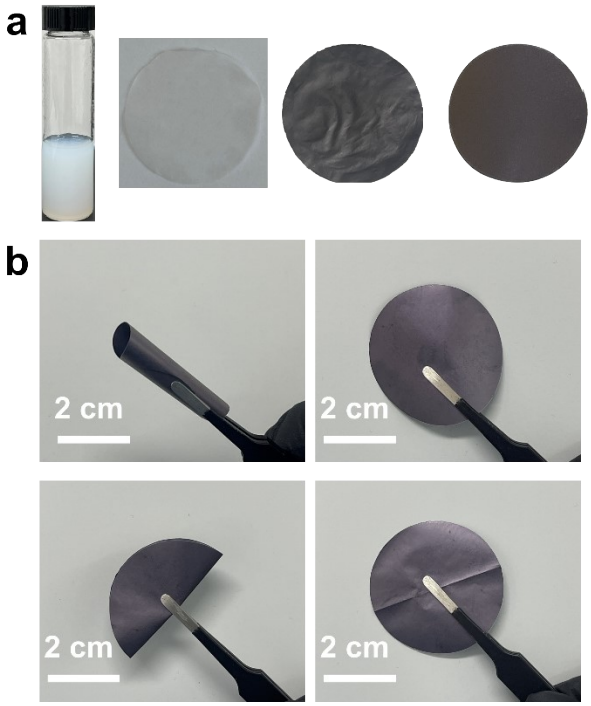

Figure S9. (a) Optical images of BC dispersion, BC film, $Ti_3C_2T_x$-NaAsc film, and $Ti_3C_2T_x$-NaAsc/BC film. (b) Optical images of $Ti_3C_2T_x$-NaAsc60%/BC films bent, rolled, folded, and unfolded.

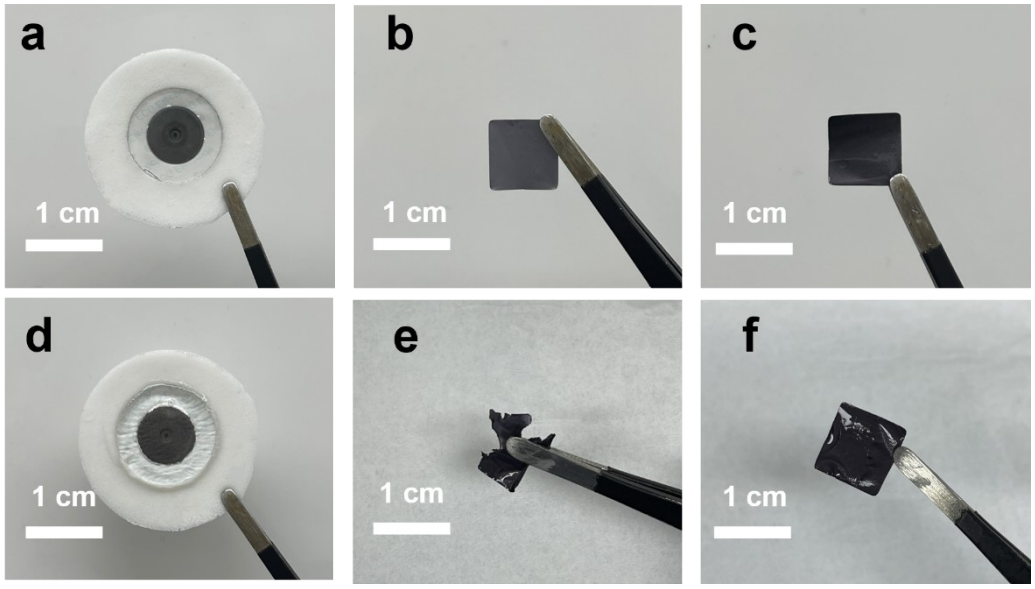

Figure S10. (a-c) Optical images of Ag/AgCl, $Ti_3C_2T_x$-NaAsc, and $Ti_3C_2T_x$-NaAsc/BC under normal conditions. (d-f) Images of Ag/AgCl, $Ti_3C_2T_x$-NaAsc, and $Ti_3C_2T_x$-NaAsc/BC after being placed in a sweat environment for 20 minutes.

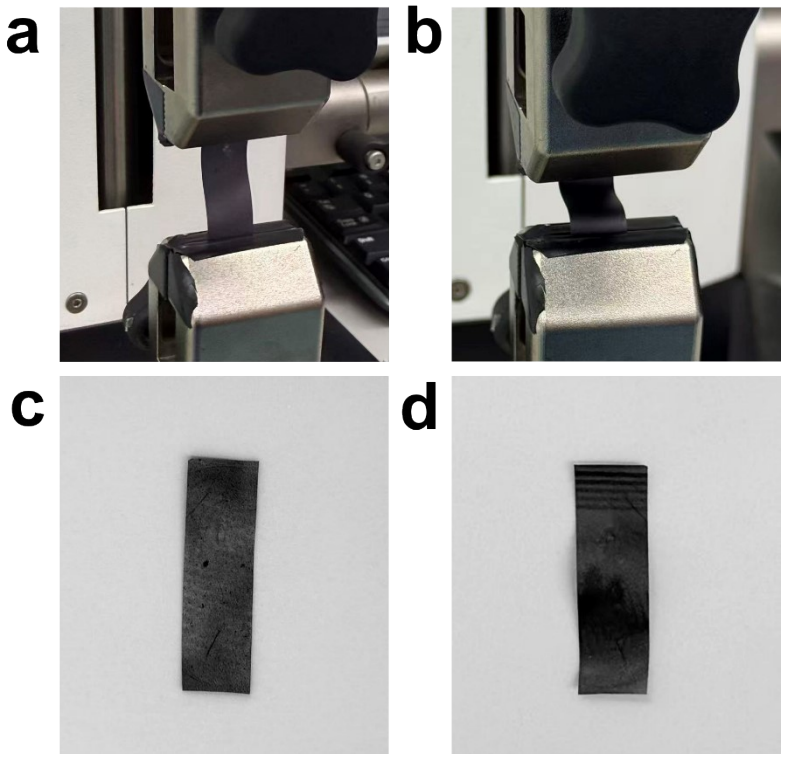

Figure S11. (a-b) Optical mages of the $Ti_3C_2T_x$-NaAsc/BC electrode before and after bending. (c-d) Optical images of the $Ti_3C_2T_x$-NaAsc/BC electrode before and after 1000 bending cycles.

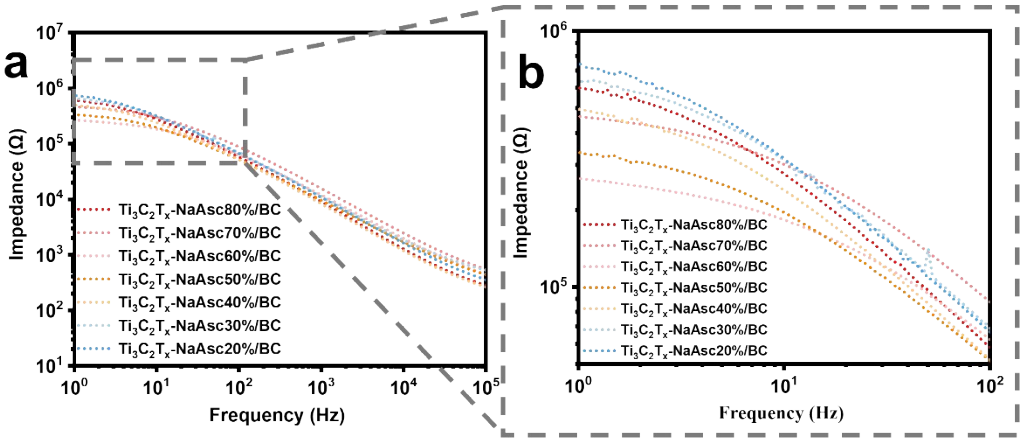

Figure S12. Skin-electrode interface impedance of $Ti_3C_2T_x$-NaAsc/BC bioelectrodes with different $Ti_3C_2T_x$-NaAsc loadings.

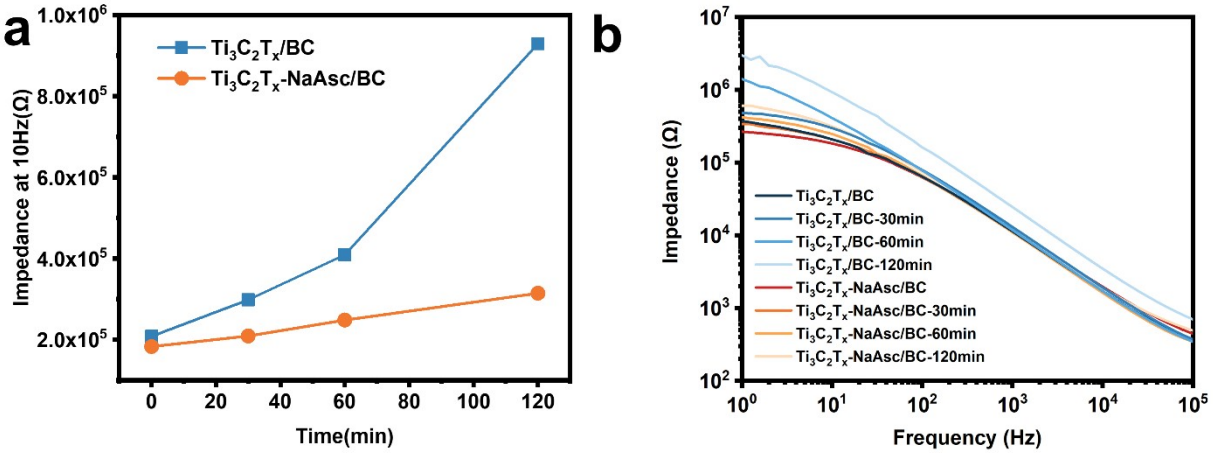

Figure S13. (a) The changes in interface impedance of $Ti_3C_2T_x$-NaAsc/BC and $Ti_3C_2T_x$/BC at 10 Hz with the increase of aging time. (b) The interface impedance of skin electrodes after different heating durations (0, 30, 60, and 120 min) from 1 to 105 Hz.

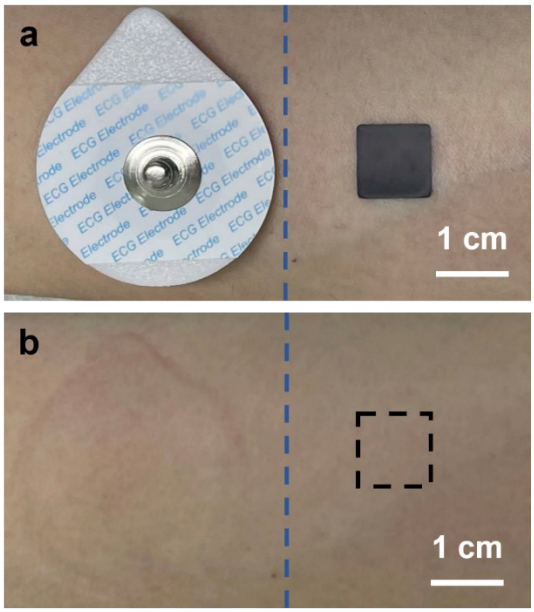

Figure S14. (a) Initial image of the Ag/AgCl gel electrode versus the $Ti_3C_2T_x$-NaAsc/BC bioelectrode on the subjects' skin. (b) Optical images the Ag/AgCl gel electrode versus the $Ti_3C_2T_x$-NaAsc/BC bioelectrode after being placed on the skin of the subjects for five hours.

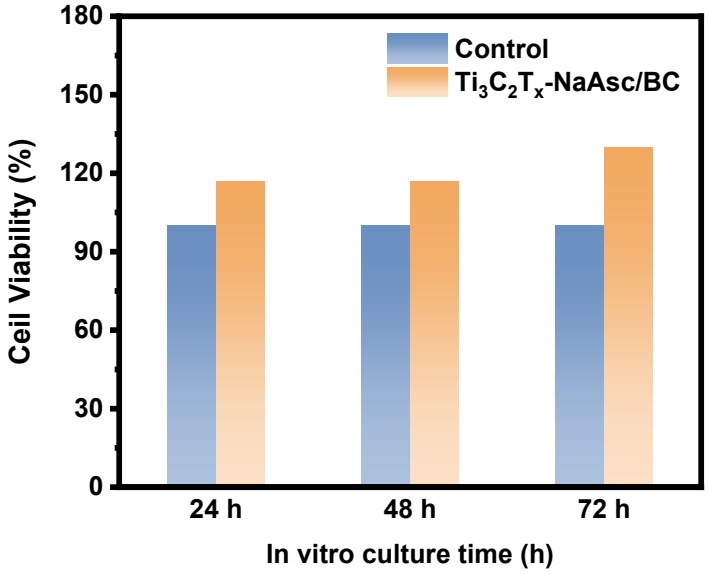

Figure S15. Live/dead stained laser confocal microscope images of Hela cells co-cultured with $Ti_3C_2T_x$-NaAsc/BC bioelectrode for 24 h and 72 h.

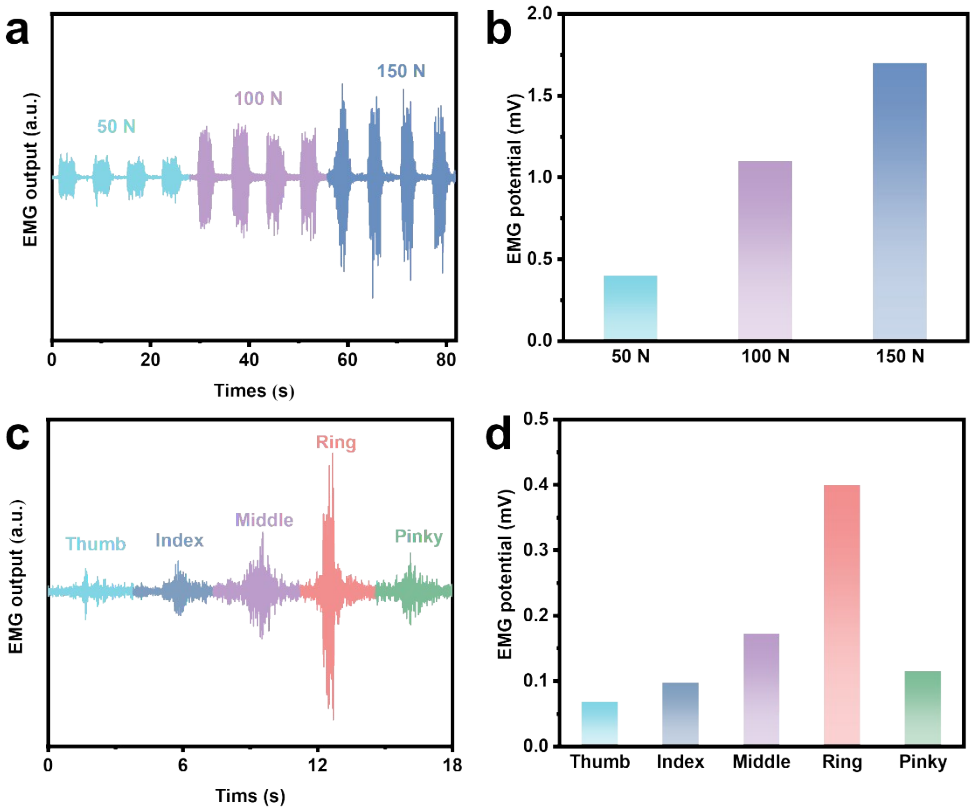

Figure S16. (a) EMG signals under different grip strengths. (b) Signal strength corresponding to EMG signals under different grip strengths. (c) EMG signals generated

with different finger flexion and extension (d) Signal strength corresponding to EMG signals generated with different finger flexion and extension.

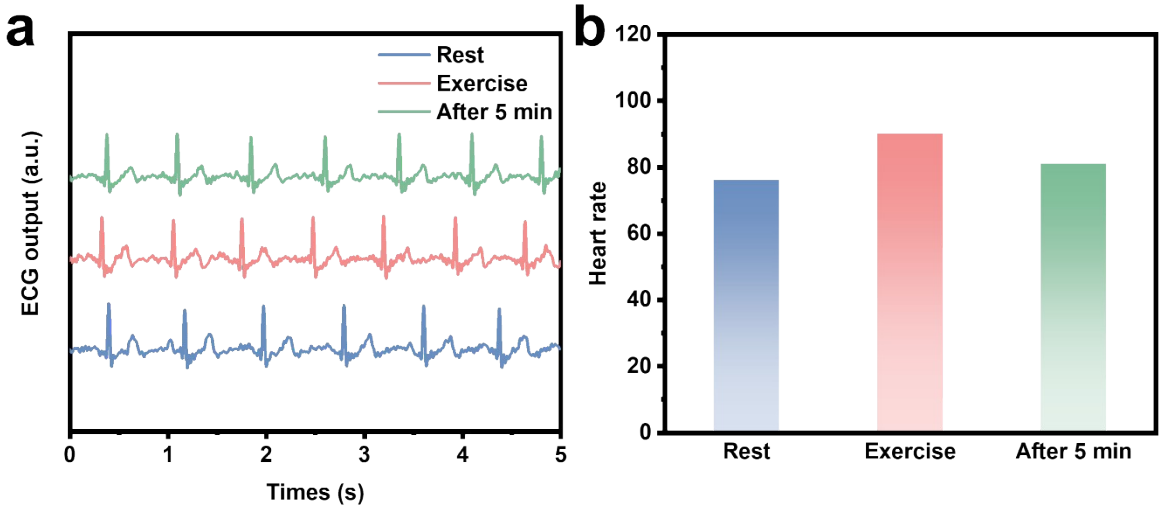

Figure S17. (a)ECG recorded from a subject during pre-exercise rest, exercise, and post-exercise recovery. (b) Corresponding heart rate values during the three phases.